Journal of Photochemistry and Photobiology A: Chemistry 207 (2009) 173–180

Contents lists available at ScienceDirect

Journal of Photochemistry and Photobiology A: Chemistry

journal homepage: www.elsevier.com/locate/jphotochem

Growth kinetics of CdS quantum dots and synthesis of their polymer nano-composites in CTAB reverse micelles

Saim Emin [a], Norihito Sogoshi [a], Seiichiro Nakabayashi [a,*], Masumi Villeneuve [a], Ceco Dushkin [a,b]

[a] Department of Chemistry, Faculty of Science, Saitama University, Shimo-Okubo 255, Saitama, 338-8570, Japan
[b] Laboratory of Nanoparticle Science and Technology, Faculty of Chemistry, University of Sofia, 1164 Sofia, Bulgaria

ARTICLE INFO

Article history:
Received 9 April 2009
Received in revised form 14 June 2009
Accepted 3 July 2009
Available online 12 August 2009

Keywords:
Quantum dots
CTAB
Bis-(trimethyldisilyl)sulfide
Growth kinetics
NMR
Nanocomposites

ABSTRACT

CdS nanocrystals were synthesized in reverse micelles of water/CTAB + 4-penten-1-ol/benzene. Changing the micellar environment varied the dynamics in the nanocrystals growths. In "pure micelles", which contained only Cd^{2+} and S^{2-} precursors, the growth was continuous under relatively fast process with the timescales of several tens of minutes. However, when monomer and cross-linker molecules were loaded in the micelles, the Ostwald ripening growth was observed under slow process with the timescales of several hours. Besides the nanocrystal growth, thermal polymerizations were conducted in the micellar system containing of monomer, sodium methacrylic acid, and cross-linker, N,N′-methylenebisacrylamide. The obtained hybrid materials containing nanocrystals embedded into polymer domains were observed by TEM.

1. Introduction

The semiconductor nanocrystals have attracted great fundamental and technological interests in the last two decades. They exhibit the quantum confinement effects when their sizes become comparable to the Bohr exciton radius, which results in an increase of the band gap energy relative to that of the bulk solid [1–3]. Among the variety of nano-sized semiconductors (quantum dots, QDs), cadmium sulfide (CdS) has been intensively studied due to the band-gap energy existing in the visible region, which is suitable for practical applications. The reverse micelle method is a wet synthetic technique for obtaining nanocrystals with defined sizes. Mostly, water-in-oil reverse micelles based on the double-tail surfactant AOT [sodium bis(2-ethylhexyl)sulfosuccinate] have been utilized as nano-reactors for the synthesis of QDs [4,5]. The growth mechanism has been reported for CdS QDs [6] and CdSe QDs [7] in AOT micelles. A single-tail surfactant, such as CTAB (cetyltrimethylammonium bromide), in combination with a co-surfactant is far less explored. Zhang et al. [8] have reported a procedure for the preparation of CdS QDs in H_2O/CTAB + hexanol/heptane reverse micelles in various sizes. The synthesis of QDs is achieved by mixing of two micelle solutions with solubilized Cd^{2+} and S^{2-} ions in the water phase. However, the temporal evolution of the QDs growth is not clear. This growth mechanism will be the topics of this article. We synthesized CdS QDs in H_2O/CTAB + pentanol/benzene and investigated the QDs growth kinetics from their temporal evolution of the absorption spectra. Moreover, upon completion of QDs growth, a thermal polymerization was conducted in the reverse micelles solutions in order to obtain nanocomposite materials. Together with CTAB, the co-surfactant, 4-penten-1-ol provided a double-chain moiety, which adsorbs on the water–oil interface and forms the inner micelle water pool, i.e., the micellar water core. The sulfur atoms were supplied from the oil phase (benzene) containing of BTMS (bis-(trimethyldisilyl)sulfide) as an organo-sulfur compound [9]. Since the halogen–silicon bond of BMTS is weaker than the carbon–silicon bond [10], BTMS released sulfur into the water pools. The BTMS hydrolysis proceeded at the surface of the micellar water core, and reacted with Cd^{2+} ions in the core. The growth kinetics of CdS QDs was investigated at different w (the molar ratio of water to CTAB).

Depending on the solubilized molecules in the micelle, we designed two types of studies.

The first series of experiments were the synthesis of CdS QDs in the absence of monomer and cross-linker molecules. The reverse micelles were loaded only with Cd^{2+} ions. Here, the QDs growth can be described in terms of a two-stage growth model [11]. At the first stage, the initial nuclei instantaneously increase due to the surface reaction. As the completion of the precursors in the micelle, a second stage follows, which involves supply of Cd^{2+} and S^{2-} ions

* Corresponding author. Tel.: +81 48 858 3617.
E-mail address: sei@chem.saitama-u.ac.jp (S. Nakabayashi).

1010-6030/$ – see front matter © 2009 Elsevier B.V. All rights reserved.
doi:10.1016/j.jphotochem.2009.07.002

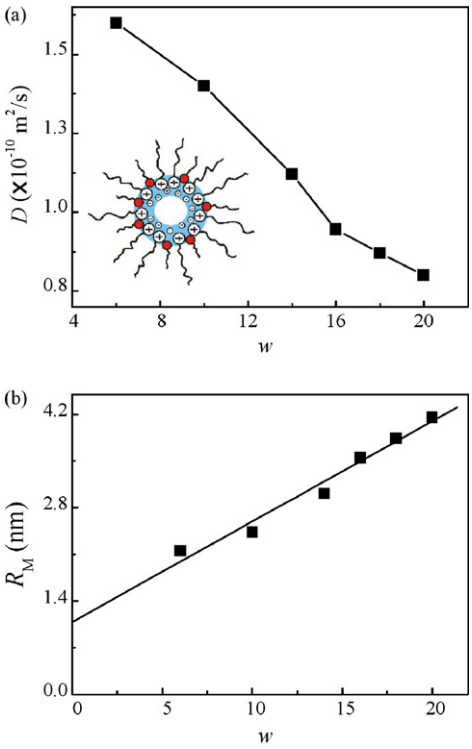

Fig. 1. (a) Plot of the self-diffusion coefficients of CTAB micelles as a function of w. (b) Plot of reverse micelle radius R_M as a function of w. The inset in the top panel shows a scheme of a reverse micelle.

from the surrounding micelles. The growth of QDs at the second stage continues until the precursors are exhausted in the overall system.

The second series of experiments were the synthesis of CdS QDs in monomer and cross-linker loaded micelles. The QDs growth was achieved in micelles, containing of Cd^{2+} ions, monomer and cross-linkers molecules. Here, some of the instantaneously formed nuclei of the QDs dissolved and progressively merged into the bigger nanocrystals. This progressive process is known as Ostwald ripening in a colloid system [12].

Further, we incorporate the nanocrystals into polymer domains by applying *in situ* polymerization at micellar stage.

2. Experimental

2.1. Sample preparation

The surfactant CTAB was re-crystallized twice in anhydrous ethanol and dried under vacuum. Benzene was dried using molecular sieves with a pore diameter of 3 Å. The dried CTAB (1.09 g) was dissolved in benzene (20 ml), and degassed water (0.32 ml) was also added. The Cd^{2+} ions were introduced as $Cd(NO_3)_2$ (concentration 0.05 M in the aqueous phase). To stabilize the reverse micelles, the co-surfactant 4-penten-1-ol (1.8 ml) was injected into the mixture. The molar ratio of 4-penten-1-ol to CTAB was adjusted at 5.5 in all the experiments. The mixture was stirred in an ultrasonic bath of power 80 W for 30 min. This allowed the formation of a transparent L2 phase (water-in-oil microemulsion) with $w = 6$. BTMS (15 μl) was quickly injected into the above dispersion. Yellow color instantaneously developed, which confirms the instantaneous QDs nucleation and growth. The ions of Cd^{2+} and S^{2-} reacted in 1:5 proportions in all samples. The QDs growth continued for about 20 min.

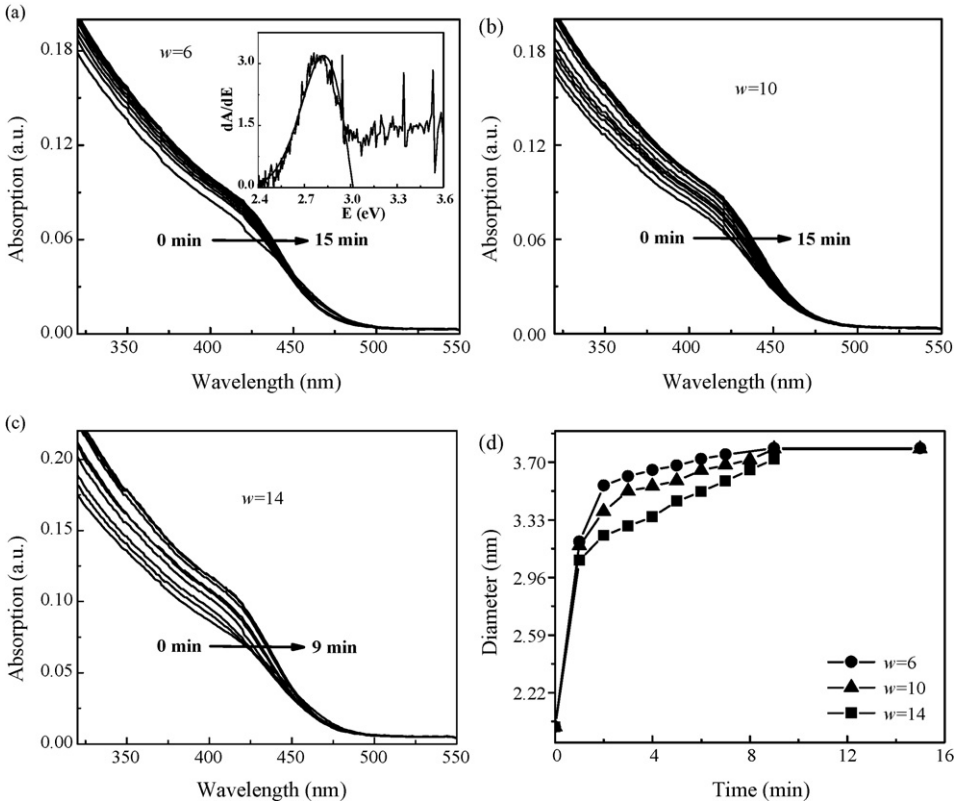

Fig. 2. Temporal changes in the absorption of light by CdS QDs synthesized in reverse micelles at various w: (a) $w = 6$; (b) $w = 10$; (c) $w = 14$; (d) sizes of CdS QDs calculated from the absorption spectra. The inset in (a) is a first differential of the absorption spectrum acquired at 9 min.

As the second experiments, i.e., the preparation of monomers and cross-linkers rich micelles, NaMA (sodium methacrylic acid) was used as a monomer and MBA (N,N′-methylenebisacrylamide) as a cross-linker. A typical procedure was as follows: CTAB (1.09 g) was dissolved in benzene (20 ml), followed by the addition of degassed water (0.32 ml) containing $[Cd^{2+}] = 0.05$ M, [NaMA] = 0.05 M and [MBA] = 0.04 M. In similar ways of the first experiments, the reverse micelles were prepared, in which the MBA concentration was adjusted at 0.09 M. The ratio w ($w = [H_2O]/[CTAB]$) was varied by changing the amount of water. BTMS (15 μl) was injected to the reverse micelle solution. The BTMS precursor was synthesized following the literature [13].

The polymerization was carried out in a flask equipped with a condenser at temperature of 45 °C, where the reaction continued for about 10 h. To activate the radical polymerization, initiator AIBN (2,2′-azobis[2-methylpropionitrile]) was used (5% v/v to NaMA). Since the initiator AIBN is known to be soluble in non-polar solvents, the polymerization would occur at the interface of oil and water.

2.2. Characterization

The diffusion coefficient of the surfactants was measured by the Pulsed-Field-Gradient-Spin-Echo (PFGSE) method using Bruker DRX spectrometer (400 MHz). In the PFGSE-NMR method, the pulsed gradient field was applied as the radio frequency pulses in a spin-echo sequence [14]. The intensity of each resonance signal decays exponentially according to the equation:

$$\frac{I(g)}{I(0)} = \exp\left[-(\gamma g\delta)^2(\Delta - \varepsilon)D\right] \quad (1)$$

where g is the square of the gradient amplitude; Δ is the Stejskal–Tanner diffusion time; D is the self-diffusion coefficient of surfactant; $I(0)$ is the proton echo intensity of $(N^+–(CH_3)_3)$ in the absence of gradient; γ is the gyromagnetic ratio (4.257×10^3 Hz G^{-1} for a proton); δ is the gradient pulse duration, and ε is the correction factor that depends on both δ and the pulse sequence used. The field gradient g was varied from 0.67 to 32 G/cm in 25 steps; the diffusion coefficient D is obtained from the semilog plot of $I(g)/I(0)$ versus g^2. The values of δ and Δ were set at 2–30 and 60–140 ms, respectively. The samples temperature was maintained at 298 K (25 °C) during the measurements.

The sizes of QDs, synthesized in NaMA and MB rich micelles, were determined from photographs obtained by transmission electron microscope (TEM) Hitachi 7500 operating at 100 kV. The absorption spectra were recorded by UV/VIS spectrophotometer, JASCO V580. The photoluminescence (PL) and photoluminescence excitation (PLE) spectra were acquired by JASCO FP6300 spectrofluorometer.

3. Results and discussion

3.1. Sizes of the reverse micelles

The surfactants diffusion coefficients were calculated from the PFGSE NMR data. An assumption was applied that the surfactants diffusion coefficients are equal to those of reverse micelles, $D_{CTAB} = D_{micelle}$ [15]. Colafemmina et al. applied similar procedures for spherical micelles as well [16]. The diffusion coefficient D of single spherical micelle is related to its radius, R_M, via the Stokes–Einstein relation [17]:

$$D = \frac{kT}{6\pi\eta R_M} \quad (2)$$

where k is the Boltzmann constant, T is the absolute temperature of sample, and η is the viscosity of solvent (medium). Fig. 1a shows a plot with the diffusion coefficients of reverse micelles as a function of w at 25 °C in d-benzene. The value of D decreased with increase in w. Further, the sizes R_M were calculated by Eq. (2) as shown in Fig. 1b versus w. The proportional relationship between R_M and w was obtained as

$$R_M(w) = 10.5 + 1.5w \quad (3)$$

Here, the intercept of 10.5 (Å) is the intrinsic (dry) CTAB micellar radius without water and the slope of 1.5 is ascribed to the increase in the water core surrounded by CTAB molecules. The slope 1.5 coincides with that reported for AOT [18].

Various methods have been applied for investigation of the micellar structures such as SANS (small-angle neutron scattering), DLS (dynamic light scattering) and PCS (photon correlation spectroscopy) [19–21]. SANS determines the water droplet radius, rather than the hydrodynamic radius of a micelle as obtained by DLS. When the water droplet radii or hydrodynamic radii are plotted as a function of w, there always appears an intercept in the plots at $w = 0$ [22]. This fact suggests that a reverse micelle has certain cavity surrounded by the surfactant heads even without addition of water (dry micelle). Trace amount of water would locate within the empty space surrounded by the surfactant heads as the inner micellar core [23]. The water trapped in the core wall is classified as "bound water", which differs from the bulk water [24,25]. Therefore, we conclude that the intercept in Fig. 1b gives the micelle inner cavity (water core), but not the surfactant tail [26]. This description coincided with the geometric model in Appendix A.

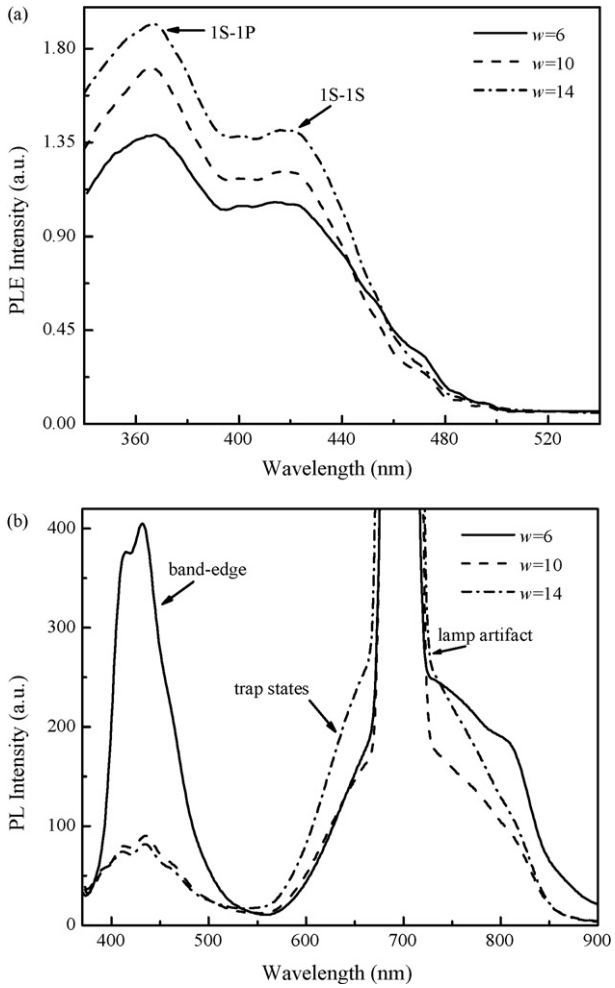

Fig. 3. CdS QDs synthesized in monomer and cross-linker free reverse micelles at various w: (a) PLE spectra (λ_{em} = 700 nm); (b) PL spectra (λ_{ex} = 350 nm).

3.2. Kinetics of the CdS nanocrystal growth in monomers and cross-linkers free micelles

The nucleation, formation of CdS QDs embryos, instantaneously occurs at the interface of the water cores in the reverse micelles after the injection of BTMS into the solution. Tiemann et al. recently reported a fast nucleation in water solutions [27] while the growth of ZnS QDs. The stopped-flow technique revealed the nucleation occurred in a timescale of milliseconds upon mixing the Zn^{2+} and S^{2-} precursors.

Similarly, in our system, the nucleation should be very fast. However, due to experimental limitations, we studied the QDs growth in the timescale of minutes. We recorded the temporal evolution of the absorption spectra by the nucleation, which occurred during the first several minutes until the Cd^{2+} and S^{2-} precursors were exhausted in the micellar water core. During the nucleation, the QDs increase their sizes relatively fast. The following growth requires an additional material supply from the nearby micelles. The QDs changed in their sizes slowly in this secondary stage. Fig. 2a–c shows the temporal evolution of the absorption spectra with different w. The edges of the absorption peak shifted toward longer wavelength with the time, which corresponds to the increase in the nanocrystal radius, R.

The QD radius, R, was calculated from the equation [28,29]:

$$\Delta E = \frac{\pi^2\hbar^2}{2R^2}\left(\frac{1}{m_e}+\frac{1}{m_h}\right) - \frac{1.8e^2}{\varepsilon R} \quad (4)$$

where m_h and m_e are the effective masses of a hole and an electron; $\varepsilon = 5.7$ is the semiconductor dielectric constant; $\hbar = 6.59 \times 10^{-16}$ (eV s) is the Planck constant; $\Delta E = E(R) - E_g$ is the difference in the band gap energy of bulk crystal E_g and that of QDs, $E(R)$. The last quantity is determined from the band-edge absorption, which corresponds to the excitonic transition 1S–1S in the QDs [30].

As shown in Fig. 2d, the diameter of nanocrystals increases rapidly at the beginning of the growth while remains nearly plateau at longer reaction times. It is obvious that the reaction proceeds faster at small w, probably due to frequent material exchange by large diffusion coefficient and large collision frequency of smaller reverse micelles. However, at the final stage of the growth, the QDs in the three samples had similar sizes. This implies that the control over QDs sizes in CTAB reverse micelles is rather insufficient compared to that in AOT micelles where the QDs sizes can be controlled by changing w. Moerover, by analyzing the CdS absorption spectra reported by Zhang et al., we found that the control over QDs sizes by varying w is poor and contrary to their statement. The discrepancy in the ir results arises due to the difference of QDs sizes obtained by TEM and those calculated from the absorption spectra. Furthermore, the absorption spectra in Ref. [8] reveals that the samples at various w exhibit quite similar sizes and coincides with the phenomenon obtained in this study.

Fig. 3a shows PLE spectra for CdS QDs grown for 20 min after the injection of BTMS into the reverse micelle solutions. In the PLE measurement, the spectrometer was set to detect the emission intensity at 700 nm as a function of the excitation photon energy.

PLE has become popular for studying thin epilayers of semiconductor films grown on opaque bulk substrates [31]. PLE experiment gave more hyperfine optical properties of the samples. The optical transition 1S–1P observed in the PLE spectra in Fig. 3a was indistinguishable in the absorption spectra in Fig. 2. The two most intensive bands in the PLE spectra are assigned to the transitions 1S–1S (at 395 nm) and 1S–1P (at 375 nm) [32], where S and P stand for the excitonic orbital in the respective QDs.

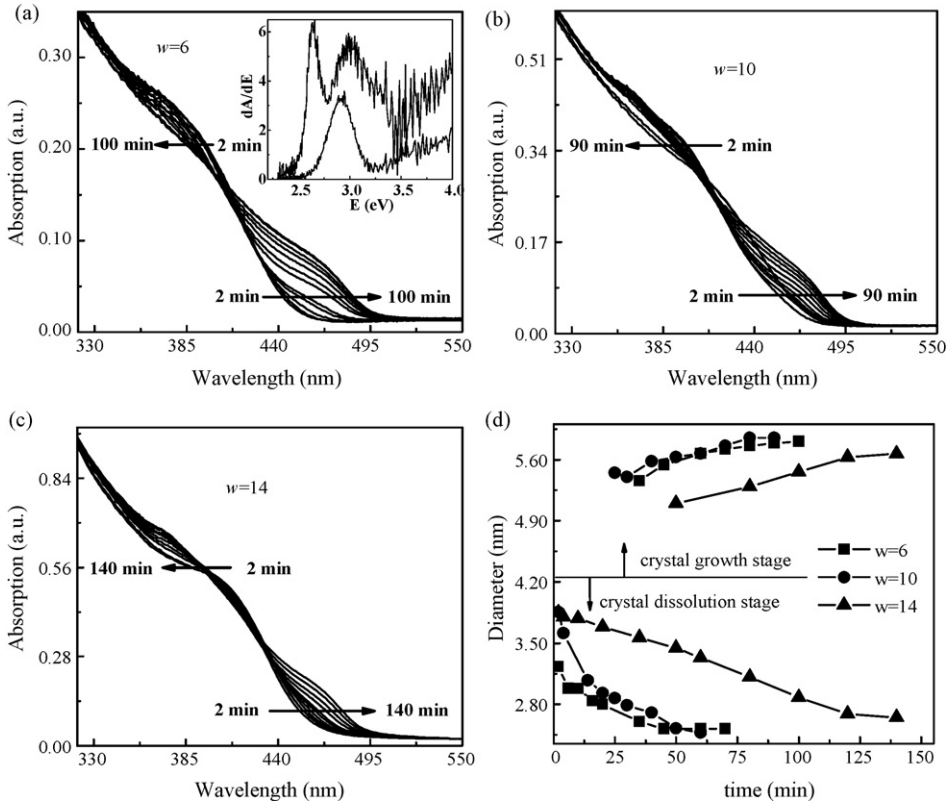

Fig. 4. Temporal changes in the absorption of CdS QDs in reverse micelles containing monomers and cross-linkers at various w: (a) $w = 6$; (b) $w = 10$; (c) $w = 14$; (d) temporal change in the sizes of CdS QDs during the Ostwald ripening, i.e., the dissolution (330 nm < λ < 385 nm) and the growth (440 nm < λ < 495 nm) of smaller and larger QDs, respectively. The inset in (a) shows the first differential of the absorption spectra acquired at 1 (lower) and 140 (higher) min. The QDs diameters were estimated by the peak wavelength at the first differential spectra.

The PLE spectra of three samples at different w did not show any significant difference as shown in Fig. 3a. This allows one concluding that the QDs synthesized at $w = 6$, 10 and 14 are of similar sizes as detected in the absorption spectra.

The quantum confinement in the QDs can also be observed by PL spectroscopy. Similar peak position obtained in the band-edge emissions in Fig. 3b show that the QDs in three samples are of the same sizes. Thus, the results from absorption, PLE and PL were consistent.

The QDs exhibited additional emissions from trap-states at longer wavelengths of about 700 nm. As seen from Fig. 3b, the PL of the specimen is overlapped with a peak coming from the second-order diffraction maximum of the excitation light (λ_{ex} = 350 nm) in the spectrometer. The trap-states related fluorescence lifetimes were of the order of 70 μs, which is surprisingly long compared to the intrinsic lifetime of the excited state of CdS QDs. Furthermore, the decay curves are shown in Appendix A.

3.3. Kinetics of CdS QDs growth in monomers and cross-linkers rich reverse micelles

The addition of monomer and cross-linker into the micellar water core induced drastic difference in the QDs growth dynamics than that obtained in the previous section. The clear Ostwald ripening mechanism was obtained.

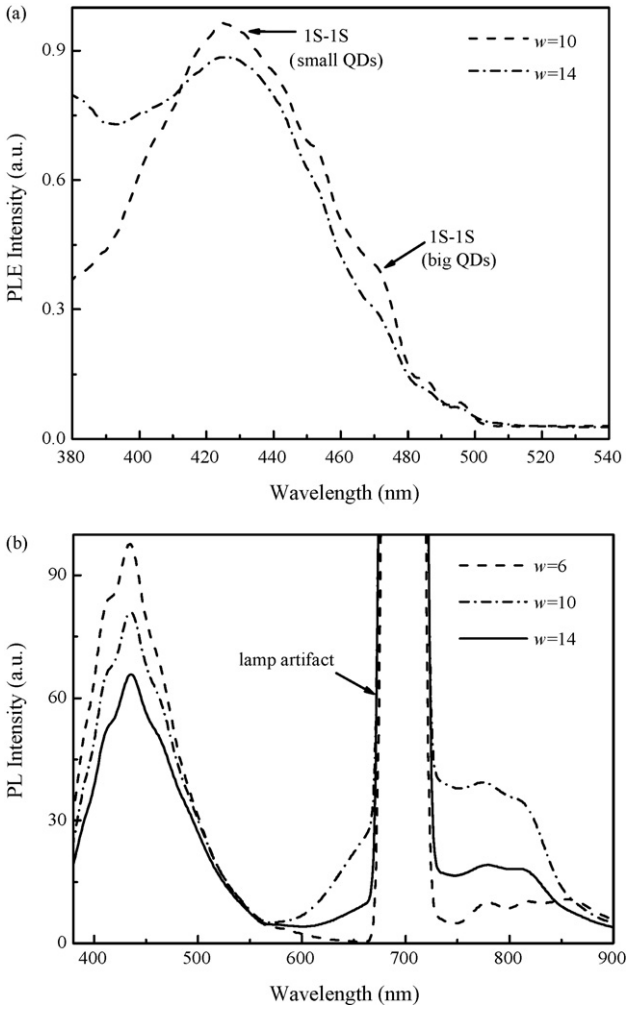

Fig. 5. CdS QDs synthesized in monomer and cross-linker rich reverse micelles at various w: (a) PLE spectra (λ_{em} = 700 nm); (b) PL spectra (λ_{ex} = 350 nm).

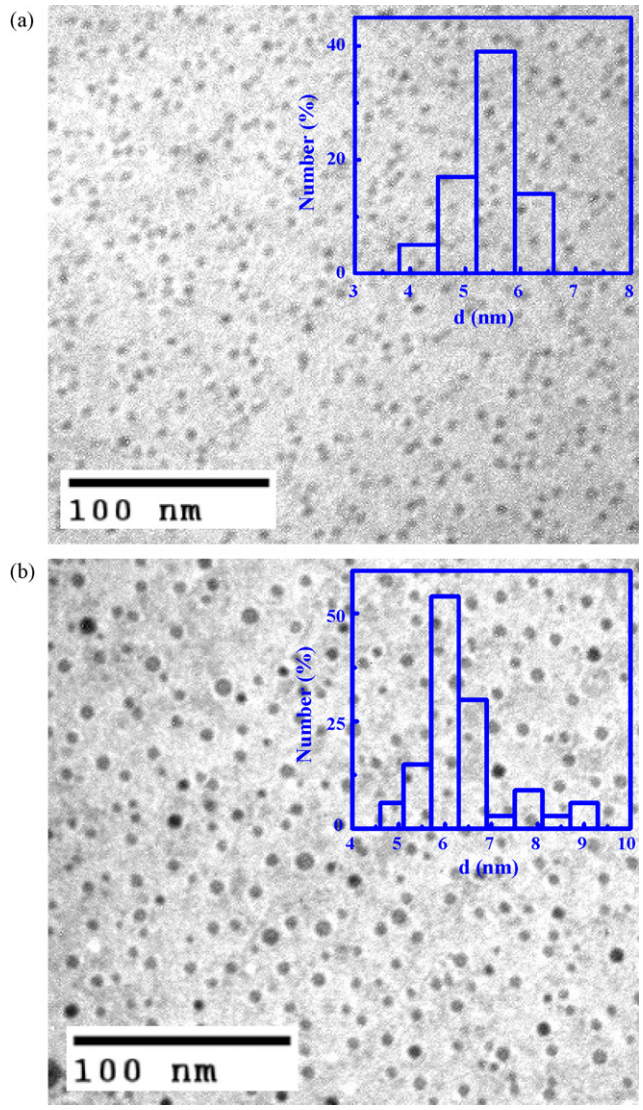

Fig. 6. TEM of CdS QDs at: (a) $w = 10$; (b) $w = 14$. The insets are the histograms with the QDs diameter.

Fig. 4 shows a series of absorption spectra of CdS QDs synthesized in monomer and cross-linker rich reverse micelles at various w. Temporal changes in the QDs absorption were given in each plot (a)–(c).

The absorption at 390 nm shifts to the shorter wavelengths with progress of the QDs growth. But, the absorption at 470 nm shifts to the longer wavelengths. These opposite shifts in the shorter and the longer wavelengths directly demonstrate that the smaller QDs are merged into the larger ones. The insets in Fig. 4a are the first differential absorption spectra at 1 and 140 min after the initiation of the growth. The single differential peak at 2.9 eV at the initial stage was divided into two at 2.6 and 3.0 eV peaks with the progress of the reaction.

Fig. 4d shows the temporal evolution of the QDs sizes, calculated from the differential absorption spectra. Two types of CdS QDs, the smaller and larger ones co-exist in the dispersion. While the smaller QDs dissolved, the larger QDs grew at the expense of ions supplied from the dissolving QDs. This process is thermodynamically driven and is known as Ostwald ripening. The micelles with the smaller w ($w = 6$ and 10) reached their steady states much rapidly than that with the larger w ($w = 14$).

Fig. 5a shows the PLE spectra of QDs samples acquired at 140 min after the injection of BTMS precursor into the solution. The inten-

sive band at 425 nm corresponds to 1S–1S transition in the smaller QDs, while the weak band at 470 nm is that in the large QDs. The size poly-dispersion makes the latter emission band broad and less intensive.

Fig. 5b shows the PL spectra of QDs taken at 140 min. Similarly with Fig. 3b, the band-edge emission of QDs at 435 nm remains unaffected by w. A broad emission from the defect states appears in these spectra as well.

PL and PLE spectra suggest that the samples synthesized at different w have quite similar QDs sizes. Moreover, the TEM images in Fig. 6 indicated the size distribution difference was not distinct between $w = 10$ and 14. The insets in each figure represent a histogram with QDs sizes. The average QDs size increases slightly from $w = 10$ to 14.

3.4. Synthesis of CdS/polymer hybrids with the combination of monomers and cross-linkers

With the completion of the QDs growth, a polymerization was initiated inside the reverse micelles. An initiator AIBN, which is soluble in the oil phase, was added into the micelle solution in order to initiate the polymerization [33]. The radical polymerization was carried out at a fixed w while changing MBA (the cross-linker) concentration. Here, MBA formed networks within the polymer chains.

The reaction allows simple incorporation of the QDs into the polymer matrix. Fig. 7 shows CdS QDs/polymer composites synthesized at $w = 14$ and different concentration of MBA. The polymerization would be the QDs in a polymer shell. The agglomerates in the images are composed of interconnected polymer shells. Each shell looks like a spherical ball as marked by the circle in the TEM image in Fig. 7b.

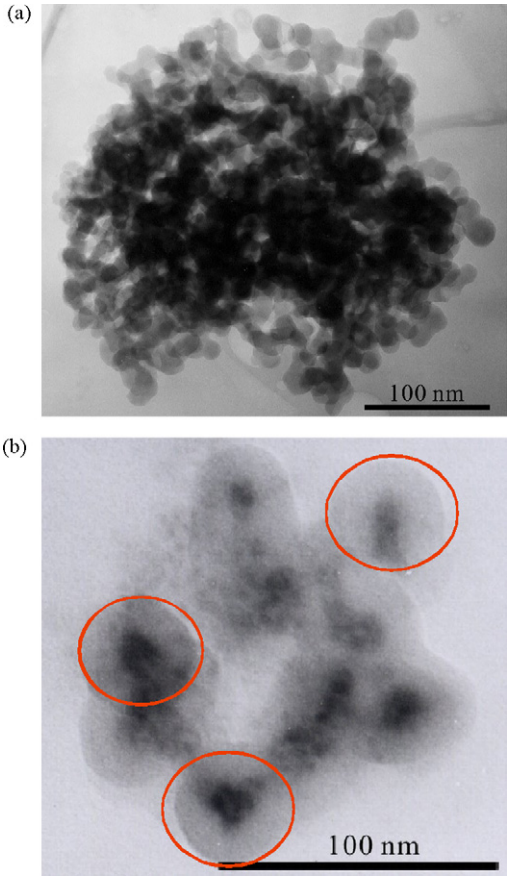

Fig. 7. TEM of CdS/polymer hybrids at: (a) [MBA] = 0.04 M; (b) [MBA] = 0.09 M.

The dark dots in the images are due to the CdS QDs, preventing the electron beam transmission through the sample. Thick polymer layers containing number of the QDs in the shells may contribute to the homogeneous dark area as well. The densely packed agglomerate of the shells appeared in dark color at the center in Fig. 7a, while the periphery was in brighter color.

A close look to this brighter area in Fig. 7a suggests that the single QDs incorporation is not so favored since low concentrations of MBA promote the QDs exchange between the micelles in the course of the polymerization. When the concentration of MBA was adjusted at 0.09 M, the incorporation of the single QDs was almost perfectly promoted as shown in Fig. 7b. Here the brighter areas correspond to thin polymer layers and the dark areas are due to the single QDs. The QDs are located at the center of each polymer shells and the agglomeration tendency between polymers was suppressed.

The procedure given here can be used also for incorporation of QDs in various polymer matrixes. Further, because the obtained nano-composite materials are water dispersible, the synthesized nano-composite will be the one of the ideal candidates for potential bio-applications such as inert and robust bio-imaging.

4. Conclusions

The kinetics of CdS QDs growth in CTAB reverse micelles was qualitatively investigated. The first series were achieved in monomer and cross-linker free micelles. The QDs growth was found to be independent of w. The second series of experiments were achieved in monomer and cross-linker rich micelles. Here, Ostwald ripening governed the QDs growth. Finally, *in situ* polymerization was conducted inside the water core in completion with the QDs growth, which is new synthetic method promising for preparation of water dispersible nano-composites.

Acknowledgements

S. Emin is thankful to the Ministry of Education, Science, Sports and Culture of Japan (Monbusho) for the granted PhD scholarship. C. Dushkin thanks to the COST D43 Action of EC and the project VUH-09/05 of the National Science Fund of Bulgaria.

Appendix A.

Here we will derive a semi-empirical equation for the dependence of water core radius R_w on the ratio w. Let us assume that initially the water, added to the system, is used to fill up the cavity of an empty (dry) micelle of radius R_0. Then the volume of this water can be expressed as

$$\frac{4}{3}\pi R_0^3 = N_0 \Omega \tag{A.1}$$

where N_0 is the number of water molecules per micelle and $\Omega = 30\ \text{Å}^3 = 3 \times 10^{-23}\ \text{cm}^3$ is the volume of a water molecule.

Further, the excess water is going to increase the micelle water radius. Let us consider a water shell of thickness Δ and volume

$$V_{\text{shell}} = \frac{4}{3}\pi(R_0 + \Delta)^3 - \frac{4}{3}\pi {R_0}^3 \tag{A.2}$$

This equation can be rearranged to give

$$V_{\text{shell}} = \frac{4}{3}\pi R_0^3 \left[\left(1 + \frac{\Delta}{R_0}\right)^3 - 1\right] \tag{A.3}$$

Assuming that the shell thickness is much smaller than R_0 ($\Delta/R_0 < 1$), Eq. (A.3) can be approximated as

$$V_{\text{shell}} \approx 4\pi R_0^2 \Delta \tag{A.4}$$

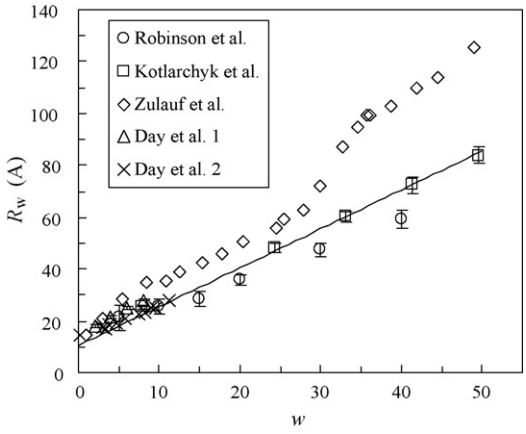

Fig. 8. Data for the micelle radius of AOT, R_w, published in literature: Robinson et al. [20], Katlarchyk et al. [22] (the data are averaged over three different temperatures), Zulauf et al. [21], and Day et al. [19] (1 and 2 are averaged over the data for two different series). The straight line is drawn by Eq. (A.13).

Hence, the volume of water core reads

$$V_w = V_0 + V_{\text{shell}} = V_0 + 4\pi R_0^2 \Delta \tag{A.5}$$

Eq. (A.5) can be rewritten as

$$N_w \Omega = N_0 \Omega + 4\pi R_0^2 \Delta \tag{A.6}$$

where N_w is the number of water molecules. This equation gives the water shell thickness

$$\Delta = \frac{(N_s w - N_0)\Omega}{4\pi R_0^2} \tag{A.7}$$

here $N_s = N_w/w$ is the number of surfactant molecules. Finally, the water core radius is expressed as

$$R_w = R_0 + \Delta \tag{A.8}$$

Replacing here Δ from Eq. (A.7), one obtains

$$R_w = R_0 - \frac{N_0 \Omega}{4\pi R_0^2} + \frac{N_s \Omega w}{4\pi R_0^2} \tag{A.9}$$

At $w = 0$, one gets from Eq. (A.9) the initial water core radius

$$R_w^0 = R_0 - \frac{N_0 \Omega}{4\pi R_0^2} \tag{A.10}$$

Inserting N_0 from Eq. (A.1) into Eq. (A.10) gives

$$R_w^0 = \frac{2}{3} R_0 \tag{A.11}$$

Then Eq. (A.9) states

$$R_w(w) = R_w^0 + \frac{N_s \Omega}{4\pi R_0^2} w \tag{A.12}$$

On the other hand, we have from the linear fit of data $R_w(w)$ that

$$R_w(w) = 10.5 + 1.5w \tag{A.13}$$

Comparing Eqs. (A.12) and (A.13) we obtain the respective quantities: $R_w^0 = 10.5$ Å , $R_0 = 3R_w^0/2 = 15.75$ Å , and

$$\frac{N_s \Omega}{4\pi R_0^2} = 1.5 \tag{A.14}$$

From Eq. (A.14) one can find the value of N_s, the number of surfactant molecules per a micelle: $N_s = 155.8$ molecules. This value is comparable with the aggregation number of AOT reverse micelles [31].

The number of water molecules per micelle follows from Eq. (A.1) $N_0 = 545.2$ molecules. Knowing N_s (which should be a constant for all micelles) and N_0, one can define the apparent w_0 corresponding to a dry micelle filled with water

$$w_0 = \frac{N_0}{N_s} \tag{A.15}$$

Replacing the respective values for N_0 and N_s one gets $w_0 = 3.5$. This value is much smaller than the value $w \approx 7$, corresponding

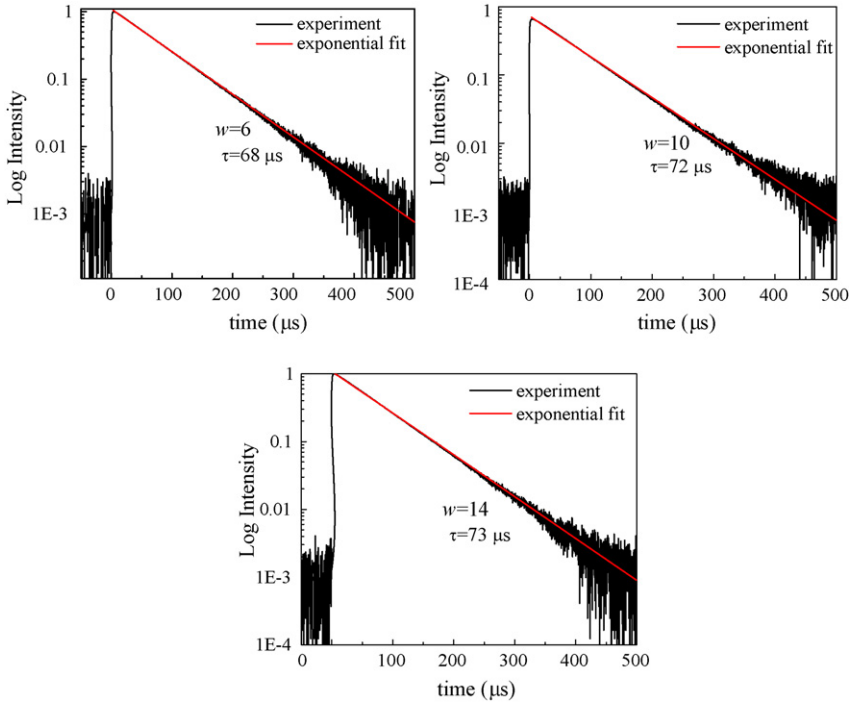

Fig. 9. Decay curves for CdS QDs defect-states emission at 700 nm measured after the injection of BTMS precursor into the micellar solution. Excitation wavelength at $\lambda_{ex} = 355$ nm.

to the transition from bound-only water to free plus bound water [32,33].

Now let us check the validity of the approximation $\Delta/R_0 < 1$. For $w = 10$ we get from Eq. (A.7), at the particular values of parameters, that $\Delta = 9.75$ Å. This gives $\Delta/R_0 = 0.62$, which justifies our assumption at least for this value of w.

Fig. 8 shows a comparison of Eq. (A.13) with the experimental data of various authors for AOT micelles.

Appendix B.

Defect state emission is detected with a band pass filter FWHM = 12 nm at 700 nm. The excitation light source for this study was Nd:YAG laser (LUMONICS), generating laser pulses with full width at half maximum (FWHM) <10 ns at 355 nm an. The laser beam intensity was 500 μJ per pulse with a repetition rate of 10 Hz. The photons are detected by photomultiplier tube (Hamamatsu H6780) with a rise time of 0.78 ns (Fig. 9).

References

[1] W.W. Yu, L. Qu, W. Guo, X. Peng, Experimental determination of the extinction coefficient of CdTe, CdSe and CdS nanocrystals, Chem. Mater. 15 (2003) 2845–2860.
[2] Y. Wang, N. Herron, Quantum size effects on the exciton energy of CdS clusters, Phys. Rev. B 42 (1990) 7253–7255.
[3] S.M. Emin, N. Sogoshi, S. Nakabayashi, T. Fujihara, C.D. Dushkin, Kinetics of photochromic induced energy transfer between manganese-doped zinc-selenide quantum dots and spiropyrans, J. Phys. Chem. C 113 (2009) 3998–4007.
[4] V.L. Colvin, A.N. Goldstein, A.P. Alivisatos, Semiconductor nanocrystals covalently bound to metal surfaces with self-assembled monolayers, J. Am. Chem. Soc. 114 (1992) 5221–5230.
[5] M.L. Steigerwald, A.P. Alivistos, J.M. Gibson, T.D. Harris, R. Kortan, A.J. Muller, A.M. Thayer, T.M. Duncan, D.C. Douglass, L.E. Brus, Surface derivatization and isolation of semiconductor cluster molecules, J. Am. Chem. Soc. 110 (1988) 3046–3050.
[6] S.M. Emin, C.D. Dushkin, S. Nakabayashi, A. Eicki, CEJC 5 (2007) 590.
[7] F.M. Pavel, R.A. Mackay, Reverse micellar synthesis of a nanoparticle/polymer composite, Langmuir 16 (2000) 8568–8574.
[8] J. Zhang, L. Sun, C. Liao, C. Yan, Size control and photoluminescence enhancement of CdS nanoparticles prepared via reverse micelle method, Solid Stat. Commun. 124 (2002) 45–48.
[9] L. Pauling, The Nature of the Chemical Bond, third ed., Cornell University Press, Ithaca, New York, 1960.
[10] K.J. Kochi, Organometallic Mechanism and Catalysis, Academic Press, New York, 1978.
[11] C.D. Dushkin, S. Saita, K. Yoshie, Y. Yamaguchi, The kinetics of growth of semiconductor nanocrystals in a hot amphiphile matrix, Adv. Colloid Interface Sci. 88 (2000) 37–78.
[12] S. Pal, G. Vishal, K.S. Gandhi, K.G. Ayappa, Ion exchange in reverse micelles, Langmuir 21 (2005) 767–778.
[13] M. Detty, M. Seidler, Bis(trialkylsilyl) chalcogenides, preparation and reduction of group VIA oxides, J. Org. Chem. 47 (1982) 1354–1356.
[14] D. Wu, A. Chen, C.S. Johnson, An improved diffusion-ordered spectroscopy experiment incorporating bipolar-gradient pulses, J. Magn. Reson. A 115 (1995) 260–264.
[15] F. Lopez, G. Palazzo, A. Ceglie, Enzymatic activity of lipase entrapped in CTAB/water/pentanol/hexane reverse micelles: a functional and microstructural investigation, Prog. Colloid Polym. Sci. 123 (2004) 174.
[16] G. Colafemmina, G. Palazzo, E. Balestrieri, M. Giomini, M. Giustini, A. Ceglie, Towards the comprehension of the cosurfactant role: a NMR self-diffusion and conductivity study of a four-components water-in-oil microemulsion, Prog. Colloid Polym. Sci. 105 (1997) 281–289.
[17] R. Zangi, L.J. Kaufman, Frequency-dependent Stokes–Einstein relation in supercooled liquids, Phys. Rev. E 75 (2007) 051501.
[18] M.P. Pileni, Reverse micelles as microreactors, J. Phys. Chem. 97 (1993) 6961–6973.
[19] R.A. Day, B.H. Robinson, J.H. Clarke, J.V. Doherty, Characterisation of water-containing reversed micelles by viscosity and dynamic light scattering methods, J. Chem. Soc., Faraday Trans. 1 75 (1979) 132–139.
[20] B.H. Robinson, C. Toprakcioglu, J.H. Dore, Small-angle neutron-scattering study of microemulsions stabilized by aerosol-OT, J. Chem. Soc., Faraday Trans. 1 80 (1984) 13–27.
[21] M. Zulauf, H.-F. Eicke, Inverted micelles and microemulsions in the ternary system H_2O/Aerosol-OT/Isooctane as studied by photon correlation spectroscopy, J. Phys. Chem. 83 (1979) 480–486.
[22] M. Kotlarchyk, S.-H. Chen, J.S. Huang, Temperature dependence of size and polydispersity in a three-component microemulsion by small-angle neutron scattering, J. Phys. Chem. 88 (1982) 3273–3276.
[23] A. Maitra, Determination of size parameters of water-aerosol OT-oil reverse micelles from their nuclear magnetic resonance data, J. Phys. Chem. 88 (1984) 5122–5125.
[24] S.M. Emin, P.S. Denkova, K.I. Papazova, C.D. Dushkin, E. Adachi, Study of reverse micelles of di isobutylphenoxyethoxyethyldimethylbenzyl ammonium methacrylate in benzene by nuclear magnetic resonance spectroscopy, J. Colloid Interface Sci. 305 (2007) 133–141.
[25] N.E. Levinger, Water in confinement, Science 298 (2002) 1722–1723.
[26] M. Giustini, G. Palazzo, G. Colafemmina, M.D. Monica, M. Giomini, A. Ceglie, Microstructure and dynamics of the water-in-oil CTAB/n-pentanol/n-hexane/water microemulsion: a spectroscopic and conductivity study, J. Phys. Chem. 100 (1996) 3190–3198.
[27] M. Tiemann, F. Marlow, J. Hartikainen, O. Weiss, M. Lindén, Ripening effect in ZnS nanoparticle growth, J. Phys. Chem. 112 (2008) 1463–1467.
[28] K. Naoe, L.G. Zimin, Y. Masumoto, Persistent spectral hole burning in semiconductor nanocrystals, Phys. Rev. B 50 (1994) 18200–18210.
[29] C.B. Murray, D.J. Norris, M.G. Bawendi, Synthesis and characterization of nearly monodisperse CdE (E = sulfur, selenium, tellurium) semiconductor nanocrystallites, J. Am. Chem. Soc. 115 (1993) 8706–8715.
[30] Z. Yu, J. Li, D.B. O'Connor, L.-W. Wang, P.F. Barbara, Large resonant stokes shift in CdS nanocrystals, J. Phys. Chem. B 107 (2003) 5670–5674.
[31] P.Y. Yu, M. Cardon, Fundamentals of Semiconductors: Physics and Material Properties, second ed., Springer, Tokyo, 1999.
[32] W. Chen, Y. Xu, Z. Lin, Z. Wang, L. Lin, Formation, structure and fluorescence of CdS clusters in a mesoporous zeolite, Sol. State Commun. 105 (1998) 129–134.
[33] H.-H. Chu, C-.S. Lin, The effect of initiators on the emulsion polymerization of 2-hydroxyethyl methacrylate, J. Polym. Res. 10 (2003) 283–287.